ACS APPLIED MATERIALS & INTERFACES

Research Article

www.acsami.org

Low-Temperature Fabrication of TiO_2 Electrodes for Flexible Dye-Sensitized Solar Cells Using an Electrospray Process

Horim Lee,[†,§] Daesub Hwang,[†,‡] Seong Mu Jo,[†] Dongho Kim,[‡] Yongsok Seo,[§] and Dong Young Kim*[,†]

[†]Optoelectronic Materials Lab, Korea Institute of Science and Technology, Seoul 136-791, Korea

[‡]Department of Chemistry, Yonsei University, Seoul 120-749, Korea

[§]Department of Materials Science and Engineering, Seoul National University, Seoul 151-744, Korea

ABSTRACT: Hierarchically structured TiO_2 (HS-TiO_2) was prepared on a flexible ITO-PEN (polyethylene naphthalate) substrate via electrospray deposition using a commercially available TiO_2 nanocrystalline powder in order to fabricate flexible DSSCs under low-temperature (<150 °C) conditions. The cell efficiency increased when using flexible ITO-PEN substrates post-treated by either a mechanical compression treatment or a chemical sintering treatment using titanium n-tetrabutoxide (TTB). The mechanical compression treatment reduced the surface area and porosity of the HS-TiO_2; however, this treatment improved the interparticle connectivity and physical adhesion between the HS-TiO_2 and ITO-PEN substrate, which increased the photocurrent density of the as-pressed HS-TiO_2 cells. The electron diffusion coefficients of the as-pressed HS-TiO_2 improved upon compression treatment, whereas the recombination lifetimes remained unchanged. An additional chemical sintering post-treatment involving TTB was tested for its effects on DSSC efficiency. The freshly coated TiO_2 submitted to TTB hydrolysis in water at 100 °C yielded an anatase phase. TTB treatment of the HS-TiO_2 cell after compression treatment yielded faster electron diffusion, providing an efficiency of 5.57% under 100 mW cm^{-2}, AM 1.5 global illumination.

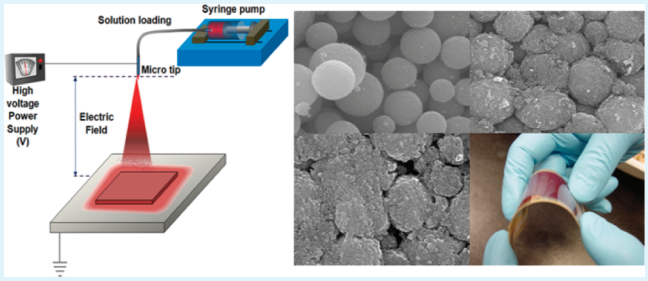

KEYWORDS: *electrospray, hierarchical structured TiO_2, flexible dye sensitized solar cells, low temperature process, compression treatment, chemical sintering*

INTRODUCTION

Dye-sensitized solar cells (DSSCs) are one of the most attractive electrochemical devices capable of converting light energy into electrical energy because they may be fabricated at low cost in an eco-friendly manner.[1] Recently, a conversion efficiency exceeding 11% under A.M 1.5G, 1 sun illumination (100 mW cm^{-2})[2−4] was achieved using Ru complex sensitizers. Plastic substrate-based flexible DSSCs have been the focus of several investigations over the past few years. Flexible DSSCs have unique advantages in their flexibility, lightweight, roll-to-roll processability, and wide applicability. Nanocrystalline TiO_2 electrodes for conventional DSSCs are usually prepared by screen-printing a TiO_2 paste containing organic binders onto an FTO glass substrate, followed by high-temperature sintering. In general, an organic binder is used to adjust the viscosity and facilitate the preparation of a TiO_2 layer of appropriate thickness. High-temperature sintering processes (>450 °C) can remove organic residues as well as sinter TiO_2 nanoparticles. The main challenge associated with the fabrication of flexible DSSCs is identifying techniques that reduce the processing temperatures because polymeric electrode substrates, such as ITO-sputtered PEN (polyethylene naphthalate) or PET (polyethylene terephthalate), undergo structural or chemical changes at higher temperatures. ITO/PEN and ITO/PET display a high transparency, are lightweight, provide a low sheet resistance, and are mechanically stable; however, their thermal stabilities are low. The development of processing techniques for fabricating photoelectrodes using polymeric flexible substrates at temperatures below 150 °C would be desirable.[5]

Several alternative approaches to the preparation of nanocrystalline TiO_2 without thermal sintering have been developed, including the transfer of TiO_2 layers,[6] doctor blading of titania paste,[7−13] electrophoretic deposition,[14−16] and spray-deposition.[17−19] Mechanical compression,[7,8] chemical sintering,[11,12,20] and microwave sintering[21] methods have been developed to introduce good connections among the as-prepared TiO_2 electrodes; however, many of these approaches are inefficient when applied to large-area fabrication techniques, and cell performances can be poor. The most critical factor underlying the low efficiency is poor interparticle connectivity among the TiO_2 particles due to absence of a thermal sintering process.

Several groups have reported zero-dimensional hierarchical structured metal oxides for the production of highly efficient glass-based DSSCs. Zero-dimensional (0D) hierarchical structured metal oxides are advantageous in that they provide (1)

Received: April 23, 2012
Accepted: June 1, 2012
Published: June 1, 2012

   dx.doi.org/10.1021/am3007164 | ACS Appl. Mater. Interfaces 2012, 4, 3308−3315

large surface areas, (2) meso- or microporous structures, (3) light scattering effects, and (4) rapid electron transport;[22−25] however, the majority of these reports have examined only glass-based conventional DSSCs fabricated through thermal sintering processes. To the best of our knowledge, few studies have reported the use of hierarchical structured TiO_2 (HS-TiO_2) for the fabrication of flexible DSSCs at room temperature.[16,18] Cha et al. described the preparation of presintered TiO_2 microballs for sinter-free processing using air-spray deposition onto flexible substrates;[18] however, the performances of DSSCs assembled using this method were poor. In addition to the poor performance, these processes were not binder-free. Organic surfactants, such as hydroxybenzoic acid, were added to the TiO_2 suspension to yield spherical microball aggregates. Chen et al. reported the room-temperature electrophoretic deposition of mesoporous TiO_2 nanoparticles to produce secondary aggregates consisting of primary anatase nanoparticles for the fabrication of flexible DSSCs.[16] Although these DSSCs performed well, the method was not practical for obtaining large-area photoelectrodes.

To overcome some limitations in low temperature fabrication of flexible DSSCs, we adopt an electrospray method that can remove the use of binders or surfactants during the process. The electrostatic spray technique has recently been considered as a cheap and simple process to directly deposit thin films from their colloidal solutions. The techniques can be applied widely in modern material technologies, microelectronics, nanotechnology.[26] During the electrospray deposition known as induction or conduction charging, the droplets can be charged of their atomization by mechanical forces in the presence of electric field between the solution and the depositing substrates.[27] The deposition efficiency of the charged droplets is usually much higher than that of the uncharged droplets, which can improve the adhesion between the materials and substrates.

We recently developed this method for the fabrication of 0D hierarchically structured TiO_2 (HS-TiO_2s) for the production of highly efficient DSSCs on FTO glass substrates. In the HS-TiO_2 structure, the electron transport was improved compared to non-HS ones.[25] The HS-TiO_2s were coated onto a flexible substrate using a binder-free dispersion of commercially available TiO_2 nanocrystalline powders (P25, Degussa). The formed HS-TiO_2s showed highly crystalline phase because the TiO_2 purity of P25 nanocrystalline powder is more than 99.5%, which consist of 70% anatase and 30% rutile. This nanocrystalline powder was, therefore, suitable for use in room-temperature fabrication methods. This method is simple and cost-effective. All processes were performed under room-temperature conditions using large-area plastic substrates. DSSCs prepared using the 0D HS-TiO_2 electrodes fabricated by electrospray displayed a high efficiency as a result of the hierarchical morphological structure of the electrode coating.

Two post-treatment techniques were tested in an effort to improve the interparticle connectivity: mechanical compression and chemical sintering using titanium n-tetrabutoxide (TTB). We characterized the effects of physical compression and optimized the conditions for fabricating highly efficient flexible DSSCs at low temperatures. Finally, we examined the performance of electrodes fabricated using TTB treatment, introduced in an effort to improve the interparticle connectivity.

EXPERIMENTAL SECTION

Materials. Indium−tin-oxide (ITO)-coated polyethylene naphthalate (PEN) (Peccell, sheet resistance 13 Ω/sq, 200 μm) was used as a transparent conducting substrate. A Pt/Ti-sputtered PEN film (Peccell, sheet resistance 5 Ω/sq) was used as a counter electrode in the flexible DSSCs. The nanocrystalline P25 powder was purchased from Degussa to prepare a TiO_2 dispersion for electrospray processing. A ruthenium complex sensitizer (Ru535-bisTBA, Solaronix SA), cis-diisothiocyanato-bis(2,2′-bipyridyl-4,4′-dicarboxylato) ruthenium(II) bis(tetrabutylammonium), generally known as N719, was purified using ion exchange column chromatography. Iodine (I_2, 99.99+%, Aldrich), 4-*tert*-butylpyridine (TBP, 99%, Aldrich), lithium iodide (LiI, 99.9%, Aldrich), 1-butyl-3-methylimidazolium iodide (BMII, 99%, C-tri), acetonitrile (ACN, 99.8%, Aldrich), valeronitrile (VN, 99.5%, Aldrich), and titanium n-tetrabutoxide (TTB, 97%, Aldrich) were used as purchased without further purification.

Preparation of the HS-TiO_2 Electrodes. The HS-TiO_2 was prepared according to the reported procedure.[25] The 10% (wt/v) P25 was dispersed in anhydrous ethanol using an ultra apex mill (Model UAM-015, Kotobuki). The stabilized P25 dispersion was loaded into a plastic syringe infusion pump (KD Scientific Model 220) connected to a high-voltage power supply (BERTAN SERIES 205B). The solution was then electrosprayed directly onto the conducting ITO-PEN film (Peccell, 13 Ω/sq, 10 cm ×10 cm). An electric field of 1.5 kV cm^{-1} was applied between the metal orifice and the conducting substrate with a feed rate of 40 μL min^{-1}. A motion control system governed by a microprocessor (Dasa Tech) was used to control the nozzle and substrate during deposition to produce a uniformly thick film over a large area.

TTB Treatment. Post-treatment with titanium n-tetrabutoxide (TTB) was implemented by soaking the as-pressed HS-TiO_2 photoelectrodes in a 0.2 M TTB/n-butanol solution for 1 h, then the photoelectrode was rinsed several times using same solution. The TTB-treated HS-TiO_2 photoelectrode was dried at room temperature for 1 h, immersed in deionized water at 100 °C for 4 h, then dried in a vacuum oven at 80 °C for 4 h. After cooling to room temperature, the TTB-treated HS-TiO_2 electrodes were immersed in a 0.3 mM N719 solution for 24 h at room temperature.

Device Fabrication. After electrospray processing, the as-sprayed HS-TiO_2 flexible photoelectrode was pressed for 10 min at 80 °C. Typical applied pressures were 10 MPa. The pressed photoelectrode was then immersed in a purified 0.3 mM N719 tert-butanol/acetonitrile (50/50 v/v) solution for 24 h at room temperature. The counter electrode was prepared by washing a Pt/Ti-sputtered PEN film with anhydrous ethanol, followed by cleaning in an ultrasonic bath containing IPA for 20 min. The dye-adsorbed HS-TiO_2 electrodes were rinsed with anhydrous ethanol and dried under a nitrogen flow. The dye-adsorbed TiO_2 electrodes were assembled and sealed along with the counter electrode using a thermal adhesive film (Surlyn, Dupont 1702, 60 μm thick) as a spacer to fabricate sandwich-type cells. The typical active area of a cell was 0.25 cm^2. The liquid electrolyte consisted of 0.65 M 1-butyl-3-methylimidazolium (BMII), 0.03 M iodine (I_2), 0.1 M lithium iodide (LiI), and 0.5 M 4-*tert*-butylpyridine (TBP) in a mixture of acetonitrile (ACN) and valeronitrile (VN) (85/15 v/v). An electrolyte solution was injected through a predrilled hole in the counter electrode.

Characterization of the Flexible DSSCs. The morphology of the HS-TiO_2 coating was investigated using a field-emission scanning electron microscopy (FE-SEM, Hitachi S-4100) with an accelerating voltage of 15 kV. The surface area and pore distribution properties were measured using a Sorptomatic 1990, the surface area was determined by the Brunauer−Emmett−Teller (BET) method, and the pore volume and size distributions were determined by the Barrett−Joyner−Halenda (BJH) method using the adsorption branches of the isotherms. The quantity of dye adsorbed onto the HS-TiO_2 surfaces was determined by desorbing the dye a 0.1 M NaOH aqueous solution, and the absorption spectra of the desorbed dye solution were measuring using a UV−vis spectrophotometer (Agilent 8453). Photovoltaic measurements of the DSSCs were conducted using an

AM 1.5 solar simulator and a 450 W Xe lamp. The intensity of the simulated light was calibrated using a Si reference solar cell to yield AM 1.5 global irradiation. The photovoltaic characteristics of the DSSC were obtained by applying an external potential bias to the cells and by measuring the photocurrent generated using a Keithley model 2400 source meter. The IPCE was measured as a function of the wavelength from 350 to 800 nm using an IPCE system designed especially for DSSCs (PV measurement, Inc.). A 75 W xenon lamp was used as the light source to generate a monochromatic beam. A NIST calibrated silicon photodiode was used as the standard during calibration. IPCE values were collected at a low chopping speed of 10 Hz. The electron transport time and electron recombination lifetime were measured by intensity-modulated photocurrent spectroscopy (IMPS) and intensity-modulated photovoltage spectroscopy (IMVS). A diode laser with variable power and modulation control (Coherent Lab-laser, 40 mW, 446 nm) was used as the light source. Illumination was always incident on the working electrode side of the solar cell. The light intensity was measured using a calibrated Si photodiode. IMVS was performed under open-circuit conditions. The output of the solar cell was connected directly to a frequency response analyzer (Schlumberger–Solartron SI 1260). IMPS measurements were performed by connecting the solar cell via a potentiostat amplifier (EG&G PAR 273) to the frequency response analyzer. During the IMPS and IMVS measurements, the cell was illuminated with sinusoidal modulated light having a small AC component (10% or less of the DC component).

RESULTS AND DISCUSSION

Morphological Changes in the HS-TiO_2 after Mechanical Compression. The electrospraying process generates microdroplets and simultaneously applies a charge by means of an electric field. SEM images of HS-TiO_2 photoelectrodes are shown in Figure 1. Hierarchically structured TiO_2 (HS-TiO_2) spherical particles with an average diameter of 600 nm were prepared via a binder-free electrospray method (Figure 1a and 1b). The individual HS-TiO_2 spherical particles consisted of P25 primary particles and were uniformly stacked on a conductive ITO-PEN substrate. The as-sprayed HS-TiO_2 spheres packed tightly in the film because of the ultrafast evaporation of the solvent during the electrospray process. Although well-structured HS-TiO_2 spheres were fabricated using the electrospray method, physical adhesion among the individual HS-TiO_2 spheres and/or the substrate was weak. The as-sprayed HS-TiO_2 films could be damaged even by weak brushing. During the electrospray process, particle stacking proceeded under the forces of the electric field and gravity. No binder materials were used during the electrospray process. Other approaches to improving the connectivity among HS-TiO_2 particles are needed. Some methods for improving interparticle connectivity have been reported, such as $TiCl_4$ treatment, but these methods are not suitable for low-temperature processing. Mechanical compression was introduced in an effort to improve particle adhesion and connectivity.

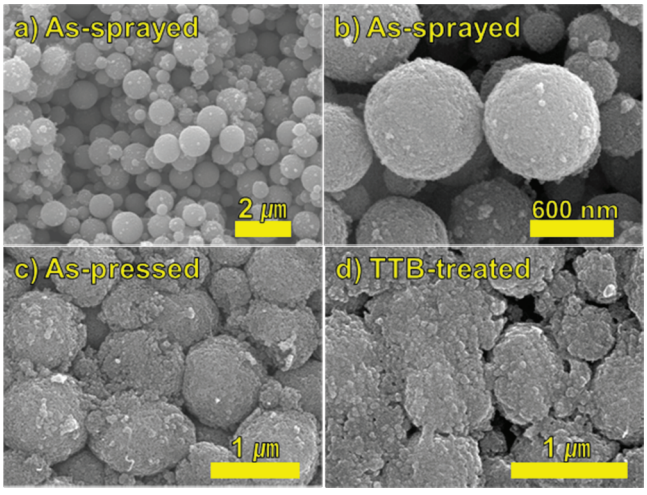

Figure 1. SEM images of (a, b) as-sprayed, (c) as-pressed, and (d) TTB-treated HS-TiO_2 photoelectrode.

Compression of the as-sprayed HS-TiO_2 photoelectrode at pressures of 10 MPa increased the HS-TiO_2 sphere interface area of the as-pressed HS-TiO_2 photoelectrodes (Figure 1c) relative to the as-sprayed HS-TiO_2 photoelectrode spheres. The morphological change after compression treatment was characterized using BJH and BET measurements.

As shown in Table 1, the pore volume of the as-pressed HS-TiO_2 was reduced from 1.36 to 0.84 $cm^3\ g^{-1}$ after compression treatment. The structures of the as-sprayed HS-TiO_2 were highly porous; however, many pores remained in the as-pressed HS-TiO_2 after compression treatment. The surface area of as-pressed HS-TiO_2 was reduced from 76.68 to 58.74 $m^2\ g^{-1}$, indicating that the interface area among the as-pressed HS-TiO_2 spheres increased upon compression treatment. The pore size distributions of the as-sprayed and as-pressed HS-TiO_2 films are shown in Figure 2. Bimodal distributions were observed for both HS-TiO_2 samples, reflecting two types of particle interface in the electrosprayed HS-TiO_2 films: the interface formed by the boundaries between primary P25 particles with micropores, and the interface formed by the boundaries between secondary HS-TiO_2 spheres with macropores. The total volume of macro-pores 100 nm in diameter was reduced, but the total volume of micropores 15 nm in diameter remained constant upon compression treatment. These results support that (1) the primary TiO_2 particles formed highly dense hierarchical structure due to the ultrafast

Table 1. Physical Characteristics of As-Sprayed and As-Pressed HS-TiO_2 Particles

HS-TiO_2 type	surface area ($m^2\ g^{-1}$)	pore volume ($cm^3\ g^{-1}$)	adsorbed dye (mol mg^{-1})
as-sprayed	76.88	1.3621	4.55×10^{-8}
as-pressed	58.74	0.8391	4.41×10^{-8}

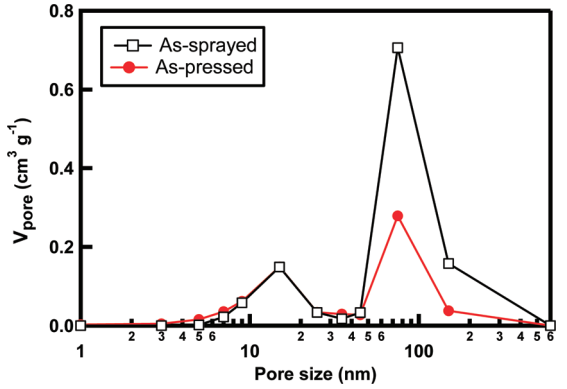

Figure 2. Pore volume distribution of as-sprayed and as-pressed HS-TiO_2 particles.

dx.doi.org/10.1021/am3007164 | ACS Appl. Mater. Interfaces 2012, 4, 3308–3315

evaporation of the solvent during the electrospray process, (2) the as-sprayed HS-TiO_2 spheres weakly adhered to their neighboring ones, and (3) the contact area between each as-pressed HS-TiO_2 spheres was enlarged through mechanical compression treatment. Also, these morphological characteristics of electrosprayed HS-TiO_2 imply that the internal electron transport within an HS-TiO_2 sphere proceed more rapidly than electron transport between adjacent HS-TiO_2 ones.

Photovoltaic Performance upon Compression Treatment. Figure 3a shows the $J-V$ characteristics of assembled

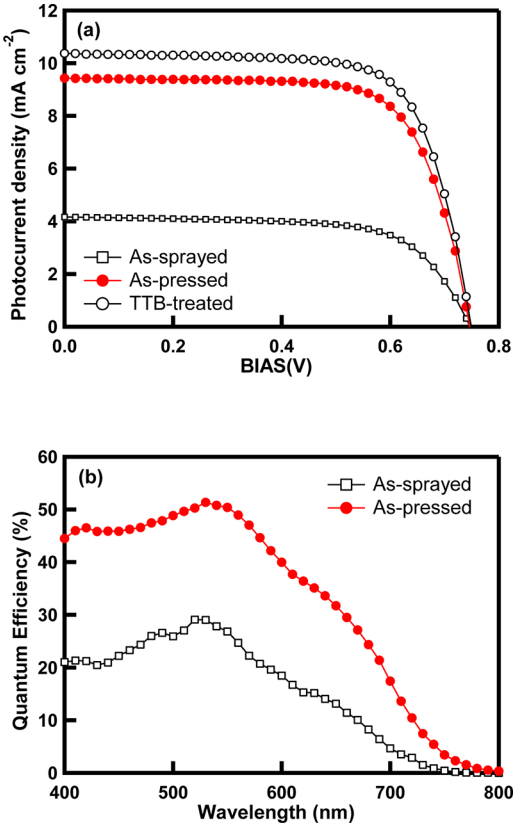

Figure 3. (a) $J-V$ curves and (b) IPCE spectra of the DSSCs based as-sprayed and as-pressed HS-TiO_2 photoelectrodes.

flexible DSSCs. The open squares and closed circles in Figure 3a indicate the $J-V$ curves associated with the as-sprayed and as-pressed HS-TiO_2 photoelectrodes, respectively. Table 2

Table 2. Photovoltaic Properties of the DSSCs Using As-Sprayed, As-Pressed, and TTB-Treated HS-TiO_2 Photoelectrode with a Film Thickness of 9 μm

HS-TiO_2 type	V_{OC} (V)	J_{SC} (mA cm^{-2})	FF	EFF (%)
as-sprayed	0.748	4.16	67.2	2.09
as-pressed	0.747	9.43	71.3	5.02
TTB-treated	0.749	10.36	71.7	5.57

summarizes the photovoltaic properties of each flexible DSSC. The conversion efficiency of the cell fabricated with the as-sprayed HS-TiO_2 film was 2.09%. The poor cell performance, particularly at a low photocurrent density, arose from the weak physical adhesion among the as-sprayed HS-TiO_2 spheres. The low fill factor of the as-sprayed HS-TiO_2 provided further evidence for the poor adhesion of the HS-TiO_2 film to the ITO-PEN substrate; however, after compression treatment, the power conversion efficiency of the as-pressed HS-TiO_2 cell increased to 5.02%. The photocurrent density increased by more than a factor of 2. The difference between the photocurrents generated by the as-sprayed and as-pressed HS-TiO_2 electrodes was investigated by measuring the incident photon-to-current conversion efficiency (IPCE). The key parameter determining the photocurrent density is the IPCE. Figure 3b shows the IPCE spectra of the as-sprayed and as-pressed HS-TiO_2 photoelectrodes. The quantum efficiency of the as-pressed HS-TiO_2 photoelectrode was higher than that of the as-sprayed HS-TiO_2 for all incident light wavelengths. Maximum IPCE values of 51 and 29% were achieved using the as-sprayed and as-pressed HS-TiO_2 photoelectrode, respectively. These results were consistent with the current density values listed in Table 2.

The IPCE depends on the light harvesting efficiency (η_{LH}), the electron injection efficiency (η_{INJ}), and the electron collection efficiency (η_{COL}). The light harvesting, electron injection, and electron collection efficiencies are related to the amount of dye adsorbed onto the TiO_2, the fraction of photons absorbed by the dye that are converted into conduction band electrons, and the degree of TiO_2 interparticle connectivity.[5] As stated above, mechanical compression affected the morphological parameters of the HS-TiO_2 particles, including the surface area and porosity. These morphological changes can alter the amount of dye adsorbed onto the HS-TiO_2 or the charge transport properties in terms of the η_{LH} or η_{COL}. The amount of dye adsorbed in the as-sprayed HS-TiO_2 film was 4.55×10^{-8} mol mg^{-1}, nearly identical to that adsorbed in the as-pressed HS-TiO_2 film (4.41×10^{-8} mol mg^{-1}), as shown in Table 1. The difference between the quantities of dye adsorbed onto the HS-TiO_2 could not explain the difference in the photocurrent generation in terms of η_{LH}. These results agreed with our previous report.[25] The other key parameter, η_{COL}, is associated with the electron diffusion coefficient and the electron recombination lifetime. As mentioned, we introduced a mechanical compression treatment to increase the interparticle connectivity and the photocurrent density levels from the low values associated with the as-sprayed HS-TiO_2. The mechanism underlying the photocurrent increase as a result of compression was investigated by measuring the charge transport properties of the as-sprayed and as-pressed HS-TiO_2 electrodes through intensity-modulated photocurrent spectroscopy (IMPS) and intensity-modulated photovoltage spectroscopy (IMVS) measurements. Figure 4 shows typical IMPS and IMVS plots of the assembled flexible DSSCs. The diffusion coefficient was calculated from the IMPS curve according to eq 1,

$$D = \frac{d^2}{2.5\tau_d} \quad (1)$$

where D, d, and τ_d are the diffusion coefficient, thickness of the TiO_2 layer, and electron transport time, respectively. The electron transport time could be estimated from the relation 2,

$$\tau_d = \frac{1}{2\pi f_{min}} \quad (2)$$

where f_{min} is the characteristic frequency at the minimum of the imaginary component of the IMPS curve (Figure 4a). The electron recombination lifetimes in the DSSCs were determined using eq 3,

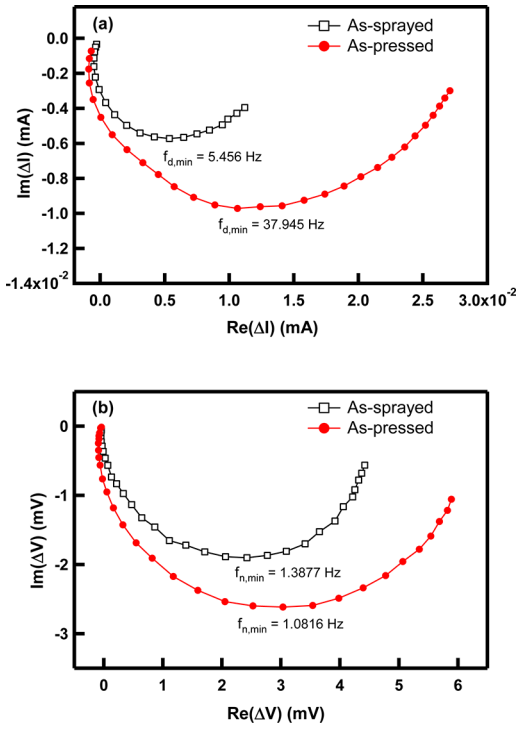

Figure 4. Typical (a) IMPS and (b) IMVS plots of the DSSCs based as-sprayed and as-pressed HS-TiO_2 photoelectrodes.

$$\tau_r = \frac{1}{2\pi f_{min}} \quad (3)$$

where f_{min} is the characteristic frequency at the minimum of the imaginary component of IMVS (Figure 4b). The calculated results are shown in Figure 5. The diffusion coefficients of the as-pressed HS-TiO_2 were 1 order of magnitude higher than those of the as-spayed HS-TiO_2 within the measured photon flux range. This IMPS result indicated that mechanical compression treatment enlarged the contact area among HS-TiO_2 spheres, and the electron diffusion properties of the HS-TiO_2 electrode improved with the mechanical compression treatment, leading to a higher photocurrent density. Figure 5b shows the recombination lifetimes of the assembled flexible DSSCs. Although the τ_r values of the as-pressed HS-TiO_2 films were slightly longer than those of the as-sprayed HS-TiO_2 films over the measured photon flux range, the difference in the recombination lifetime was insignificant and could not explain the higher photocurrent density after compression treatment. It was concluded that the higher photocurrent density did not arise from the longer recombination lifetimes, but rather from the faster electron transport (i.e., a larger electron diffusion coefficient). Morphologically, the average electron transport path length in the as-pressed HS-TiO_2 was shorter than that in the as-sprayed HS-TiO_2 film for an equal TiO_2 film weight because the as-pressed HS-TiO_2 particles were more dense (i.e., less porous) in structure. The structural features of the as-pressed HS-TiO_2 films facilitated rapid electron diffusion and generated a high photocurrent.

Thickness Dependence of the As-Pressed HS-TiO_2 Photoelectrodes. The optimum thickness of the as-pressed HS-TiO_2 photoelectrodes was determined by measuring the efficiency parameters of the cell as a function of the thickness, from 3 to 21 μm. Figure 6 and Table 3 show the photovoltaic performances of DSSCs prepared with photoelectrodes with as-

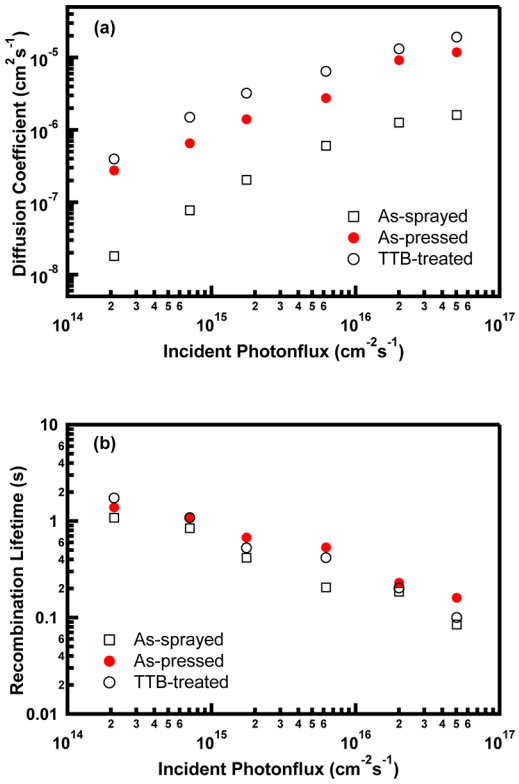

Figure 5. (a) Electron diffusion coefficient and (b) recombination lifetime of the DSSCs based as-sprayed, as-pressed, and TTB-treated HS-TiO_2 photoelectrodes as a function of the incident photonflux for 446 nm modulated (<10%) laser illumination.

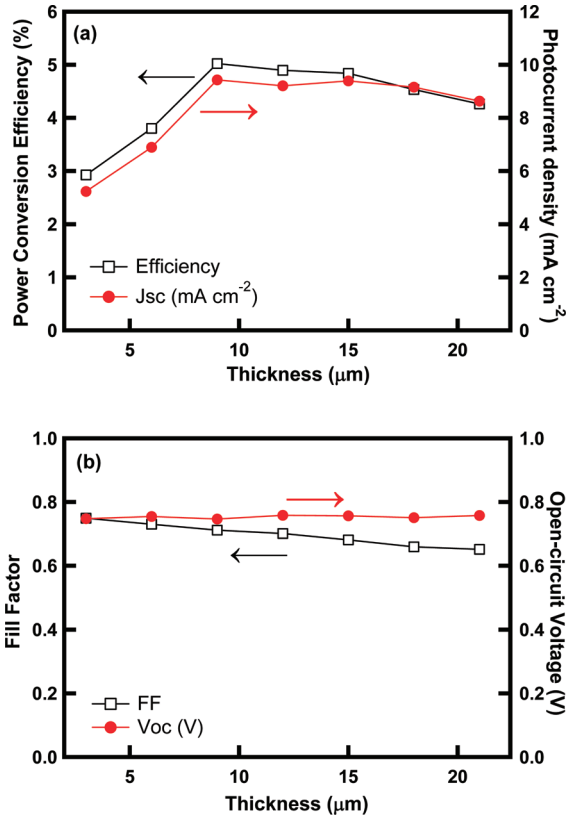

Figure 6. Photovoltaic properties of DSSCs prepared with photoelectrodes with as-pressed HS-TiO_2 films of various thicknesses.

dx.doi.org/10.1021/am3007164 | ACS Appl. Mater. Interfaces 2012, 4, 3308−3315

Table 3. Summary of Photovoltaic Performance of DSSC Prepared with Photoelectrode with As-Pressed HS-TiO_2 Films of Various Thickness

thickness (μm)	3	6	9	12	15	18	21
V_{OC} (V)	0.748	0.755	0.747	0.759	0.757	0.751	0.758
J_{SC} (mA cm^{-2})	5.23	6.89	9.43	9.21	9.39	9.16	8.63
FF	74.3	73.1	71.3	70.1	68.1	66.0	65.1
EFF (%)	2.93	3.80	5.02	4.90	4.84	4.53	4.26

pressed HS-TiO_2 films of various thicknesses. The photoelectrode thicknesses were easily controlled by adjusting the electrospray deposition time. All sample thickness values were measured after compression treatment using a surface profiler. In general, the total amount of adsorbed dye was proportional to the thickness of the photoelectrode; therefore, as the thickness of the as-pressed HS-TiO_2 increased, the photocurrent density and conversion efficiency increased. The conversion efficiency of the as-pressed HS-TiO_2 cell reached its highest value of 5.02% at 9 μm; however, beyond 9 μm, the photocurrent density and conversion efficiency decreased slightly. This trend was observed because the electron pathway from the top of the photoelectrode to the conducting substrate was too long to permit transport without recombination. The open circuit voltages of the as-pressed HS-TiO_2 photoelectrodes were constant over the range of measured thickness values, and the fill factors of the as-pressed HS-TiO_2 decreased continuously. The decrease in the fill factor as the thickness increased resulted from an increase in the resistance of the thick HS-TiO_2 electrode. The DSSC photovoltaic performances for the various photoelectrode thicknesses are summarized in Table 3.

The optimum thickness was quantitatively analyzed by calculating the electron diffusion length (L_n) using the measured IMPS and IMVS results, according to eq 4

$$L_n = \sqrt{D_n \tau_r} \tag{4}$$

where D_n and τ_r are the diffusion coefficient and recombination lifetime of electrons, respectively. The electron diffusion length represents the average distance that injected electron can travel through a photoelectrode prior to recombination. This relation implies that the electron diffusion length, L_n, should be longer than the thickness of the photoelectrode in order to effectively collect the photocurrent. The calculated average L_n of the as-pressed HS-TiO_2 film was 10.77 μm, longer than the optimum thickness (9 μm) of the as-pressed HS-TiO_2 photoelectrode. For this reason, the optimum efficiency occurred at a thickness of 9 μm, and the conversion efficiency of the as-pressed HS-TiO_2 cells decreased above a thickness of 12 μm.

TTB-Treatment after Compression Treatment. As mentioned, the low efficiency of the as-sprayed HS-TiO_2 films was overcome and well-structured HS-TiO_2 photoelectrodes were prepared by introducing a physical post-treatment. The mechanical compression treatment improved the physical interparticle necks of the HS-TiO_2 spheres, as well as the electron transport properties, which increased the photocurrent density of the cells. Although a higher efficiency was achieved using this physical treatment of the as-pressed HS-TiO_2 electrodes, further improvements were achieved by introducing chemical post-treatments using a titanium precursor.

Conventional FTO-based DSSCs include a preparation step involving a chemical post-treatment using, for example, $TiCl_4$[25,31,32] or TTIP,[33] which improved the conversion efficiency of the as-prepared photoelectrodes. Our group reported conversion efficiency improvements using $TiCl_4$ treatment of the HS-TiO_2 films in conjunction with a thermal sintering process;[25] however, these chemical post-treatments were not suitable for plastic-based flexible DSSCs because a high-temperature thermal treatment process was necessary to crystallize the as-treated titanium precursor. Moreover, the ITO-PEN surface could be corroded under acidic conditions during the $TiCl_4$ treatment. Alternative low-temperature processing approaches must be tested for the fabrication of flexible DSSCs. In this research, titanium n-tetrabutoxide (TTB) treatment was introduced to improve the HS-TiO_2 interparticle physical necks. Recently, Fan et al. used TTB as a sintering medium under ambient atmospheric conditions to prepare flexible DSSCs;[28] however, this method was unfavorable for electron transport applications because the product of TTB hydrolysis under such conditions is amorphous.[28,29] Tan et al. reported that a hydrothermal reaction of TTB with water at 100 °C under atmospheric pressure induced formation of a crystalline anatase TiO_2.[30] Therefore, we applied this method to fabricate crystalline TiO_2 because the hydrothermal conditions were suitable for flexible substrates. Hot water treatment of TTB was implemented by immersing air-dried TTB-treated photoelectrodes in 100 °C water for 4 h to crystallize the amorphous TTB into an anatase phase. Prior to the post-treatment of TTB, XRD patterns of the air-dried TTB and hot water-treated TTB were investigated. The air-dried TTB was amorphous, but the hydrolyzed phase of the hot water-treated TTB was anatase, as shown in Figure 7. This indicated that the newly formed anatase phase from the hot water-treated TTB could assist electron transport among the HS-TiO_2 spheres, unlike the amorphous air-dried TTB.

Figure 1d shows an SEM image of the TTB-treated HS-TiO_2 electrode. Each as-pressed HS-TiO_2 sphere was well-connected by the hydrolyzed TTB. The anatase coating, newly introduced by hydrolysis of the TTB layer on the as-pressed HS-TiO_2 spheres, improved the interparticle connectivity, which improved electron transport through the as-pressed HS-TiO_2

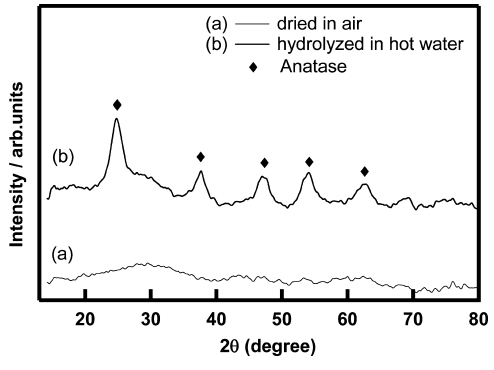

Figure 7. XRD diffraction patterns of (a) air-dried TTB and (b) hot water-treated TTB.

dx.doi.org/10.1021/am3007164 | ACS Appl. Mater. Interfaces 2012, 4, 3308−3315

photoelectrode. The J−V curves of the TTB-treated cell and as-pressed cell are illustrated in Figure 3a, and the photovoltaic parameters of these cells are summarized in Table 2. As mentioned above, the best efficiency achieved for the as-pressed HS-TiO_2 photoelectrodes was 5.02%. The V_{OC} and FF of TTB-treated cells were comparable to the values of the as-pressed cell, whereas a higher conversion efficiency of η = 5.57% was obtained in conjunction with a higher photocurrent density. This higher photocurrent density could be interpreted as improved interparticle connectivity among the HS-TiO_2 spheres. Panels a and b in Figure 5 show the diffusion coefficients and recombination lifetimes of the as-pressed HS-TiO_2 and TTB-treated HS-TiO_2 cells, calculated from IMPS and IMVS measurements in an effort to investigate the mechanism underlying the photocurrent improvement. The diffusion coefficients of the TTB-treated HS-TiO_2 electrode were higher across all measured photon flux ranges compared with those of the as-pressed HS-TiO_2 electrode. The rapid electron transport was consistent with a higher photocurrent density in the TTB-treated HS-TiO_2 electrodes; however, the recombination lifetime of the TTB-treated TiO_2 was indistinguishable from the corresponding value in the as-pressed HS-TiO_2 electrodes. Unlike general chemical treatments, such as $TiCl_4$,[31,32] the TTB treatment could not retard the recombination rate of the injected electrons. This result indicated that the TTB treatment could not change the TiO_2 conduction band edge or the surface state, although it facilitated electron diffusion through the new anatase TiO_2 coating.

CONCLUSION

In this study, we proposed a new simple fabrication process for preparing flexible DSSCs at room temperature. We prepared HS-TiO_2 photoelectrodes using an electrospray method with a binder-free TiO_2 dispersion. The HS-TiO_2 film formed by this method yielded a large surface area and a highly porous structure. The conversion efficiency of the as-sprayed HS-TiO_2 particles on the plastic ITO-PEN substrate was poor due to poor interparticle connectivity among the as-sprayed HS-TiO_2 spheres. Two post-treatments were tested in an effort to enhance the interparticle connectivity. First, we mechanically compressed the films to form physically well-connected HS-TiO_2 structures. The conversion efficiency improved by a factor of 2 using this method. By optimizing the thickness of the photoelectrode and the compression conditions, the conversion efficiency of the flexible DSSCs reached a value of 5% for the as-pressed HS-TiO_2 photoelectrodes. An additional TTB low-temperature chemical treatment was applied, yielding highly efficient flexible DSSCs. The resulting TTB-treated HS-TiO_2 photoelectrode displayed rapid electron transport, resulting in a maximum conversion efficiency of 5.57% under 1 sun illumination (100 mW cm^{-2}). This simple, cost-effective electrospray method using two types of post-treatment shows promise for the fabrication of highly efficient flexible DSSCs.

AUTHOR INFORMATION

Corresponding Author

*E-mail: dykim@kist.re.kr. Tel: +82-2-958-5323. Fax: +82-2-958-5309.

Notes

The authors declare no competing financial interest.

ACKNOWLEDGMENTS

The authors gratefully acknowledge the support from the KIST Institutional Programs (Project 2E22831 and 2K01970) (DYK), World Class University Programs (*R*32-2010-000-10217; the Ministry of Education, Science and Technology, Korea (MEST)) (D.K.), and Basic Research Program (RIAM 041-2004-I-D00224; the Korea Research Foundation) and Fundamental R&D Program for Core Technology of Materials (RIAM 0417-20100043; MOCIE) (Y.S.).

REFERENCES

(1) O'regan, B.; Gratzel, M. *Nature* **1991**, *353*, 737−740.
(2) Chiba, Y.; Islam, A.; Watanabe, Y.; Komiya, R.; Koide, N.; Han, L. *Jpn. J. Appl. Phys* **2006**, *45*, 638−640.
(3) Gratzel, M. *Inorg. Chem.* **2005**, *44*, 6841−6851.
(4) Nazeeruddin, M. K.; De Angelis, F.; Fantacci, S.; Selloni, A.; Viscardi, G.; Liska, P.; Ito, S.; Takeru, B.; Gratzel, M. *J. Am. Chem. Soc.* **2005**, *127*, 16835−16847.
(5) Toivola, M.; Halme, J.; Miettunen, K.; Aitola, K.; Lund, P. D. *Int. J. Energy Res.* **2009**, *33*, 1145−1160.
(6) Durr, M.; Schmid, A.; Obermaier, M.; Rosselli, S.; Yasuda, A.; Nelles, G. *Nat. Mater.* **2005**, *4*, 607−611.
(7) Yamaguchi, T.; Tobe, N.; Matsumoto, D.; Nagai, T.; Arakawa, H. *Sol. Energy Mater. Sol. Cells* **2010**, *94*, 812−816.
(8) Boschloo, G.; Lindstrom, H.; Magnusson, E.; Holmberg, A.; Hagfeldt, A. *J. Photochem. Photobiol., A* **2002**, *148*, 11−15.
(9) Zhang, D.; Yoshida, T.; Furuta, K.; Minoura, H. *J. Photochem. Photobiol., A* **2004**, *164*, 159−166.
(10) Miyasaka, T.; Ikegami, M.; Kijitori, Y. *J. Electrochem. Soc.* **2007**, *154*, A455−A461.
(11) Li, X.; Lin, H.; Li, J.; Wang, N.; Lin, C.; Zhang, L. *J. Photochem. Photobiol., A* **2008**, *195*, 247−253.
(12) Kim, K.; Lee, G. W.; Yoo, K.; Kim, D. Y.; Kim, J. K.; Park, N. G. *J. Photochem. Photobiol., A* **2009**, *204*, 144−147.
(13) Zhang, D.; Yoshida, T.; Oekermann, T.; Furuta, K.; Minoura, H. *Adv. Funct. Mater.* **2006**, *16*, 1228−1234.
(14) Yum, J. H.; Kim, S. S.; Kim, D. Y.; Sung, Y. E. *J. Photochem. Photobiol., A.* **2005**, *173*, 1−6.
(15) Grinis, L.; Kotlyar, S.; Ruhle, S.; Grinblat, J.; Zaban, A. *Adv. Funct. Mater.* **2010**, *20*, 282−288.
(16) Chen, H. W.; Liang, C. P.; Huang, H. S.; Chen, J. G.; Vittal, R.; Lin, C. Y.; Kevin, C. W. W.; Ho, K. C. *Chem. Commun.* **2011**, *47*, 8346−8348.
(17) Fujimoto, M.; Kado, T.; Takashima, W.; Kaneto, K.; Hayase, S. *J. Electrochem. Soc.* **2006**, *153*, A826−A829.
(18) Cha, S. I.; Koo, B. K.; Hwang, K. H.; Seo, S. H.; Lee, D. Y. *J. Mater. Chem.* **2011**, *21*, 6300−6304.
(19) Li, X.; Zhang, Y.; Zhang, Z.; Zhou, J.; Song, J.; Lu, B.; Xie, E.; Lan, W. *J. Power Sources* **2010**, *196*, 1639−1644.
(20) Park, N. G.; Kim, K. M.; Kang, M. G.; Ryu, K. S.; Chang, S. H.; Shin, Y. J. *Adv. Mater.* **2005**, *17*, 2349−2353.
(21) Uchida, S.; Tomiha, M.; Takizawa, H.; Kawaraya, M. *J. Photochem. Photobiol., A* **2004**, *164*, 93−96.
(22) Chou, T. P.; Zhang, Q.; Fryxell, G. E.; Cao, G. *Adv. Mater.* **2007**, *19*, 2588−2592.
(23) Chen, D.; Huang, F.; Cheng, Y. B.; Caruso, R. A. *Adv. Mater.* **2009**, *21*, 2206−2210.
(24) Kim, Y. J.; Lee, M. H.; Kim, H. J.; Lim, G.; Choi, Y. S.; Park, N. G.; Kim, K.; Lee, W. I. *Adv. Mater.* **2009**, *21*, 3668−3673.
(25) Hwang, D.; Lee, H.; Jang, S.-Y.; Jo, S. M.; Kim, D.; Seo, Y.; Kim, D. Y. *ACS Appl. Mater. Interfaces* **2011**, *3*, 2719−2725.
(26) Jaworek, A. *J. Mater. Sci.* **2007**, *42*, 266−297.
(27) Jaworek, A. *Powder Technol.* **2007**, *176*, 18−35.
(28) Fan, K.; Peng, T.; Chen, J.; Dai, K. *J. Power Sources* **2010**, *196*, 2939−2944.
(29) Park, N. G.; Van de Lagemaat, J.; Frank, A. *J. Phys. Chem. B* **2000**, *104*, 8989−8994.

(30) Tan, W.; Chen, J.; Zhou, X.; Zhang, J.; Lin, Y.; Li, X.; Xiao, X. *J. Solid State Electrochem.* **2009**, *13*, 651−656.
(31) Sommeling, P. M.; O'Regan, B. C.; Haswell, R. R.; Smit, H. J. P.; Bakker, N. J.; Smits, J. J. T.; Kroon, J. M.; van Roosmalen, J. A. M. *J. Phys. Chem. B* **2006**, *110*, 19191−19197.
(32) O'Regan, B. C.; Durrant, J. R.; Sommeling, P. M.; Bakker, N. J. *J. Phys. Chem. C* **2007**, *111*, 14001−14010.
(33) Li, Y.; Lee, W.; Lee, D. K.; Kim, K.; Park, N. G.; Ko, M. J. *Appl. Phys. Lett.* **2011**, *98*, 103301(1)−103301(3).